Estimating the fundamental frequency of a sand tailings dam using the H/V spectral ratio method

César Pastén[1]

[1]*University of Chile, Department of Civil Engineering and Advanced Mining Technology Center, Av. Blanco Encalada 2002 Of 431, Santiago, Chile*

ABSTRACT

This study estimates the fundamental frequency of an 85 m height sand tailings dam in Central Chile using the single-station Horizontal-to-Vertical H/V Spectral Ratio Method (HVSR), calculated from seismic ambient noise and earthquake records. The dam was constructed by compacting hydraulically deposited sands classified from integral copper tailings, following the downstream construction method. A proper estimate of the dam fundamental frequency is critical for evaluating its seismic response and secure the safe tailings containment when subjected to intense ground motions generated by interface and intraslab earthquakes. Results from the HVSR method are compared with those of the Standard Spectral Ratio method (SSR) calculated as the ratio of the response of the dam crest and that recorded at the dam toe. The fundamental frequency of the dam is about 0.9 Hz in the dam central part away from the abutments, but differences in the vibration frequency are identified along the downstream slope and along the crest axis from the north to south abutment. An analytical relationship between the dam fundamental frequency, the dam height, and the shear wave velocity (Vs) profile is validated.

Keywords: H/V Spectral Ratio, Standard Spectral Ratio, Tailings Dam, Fundamental Frequency.

1. Introduction

The concentration process of copper sulfide ore generates large amounts of tailings that must be safely stored in Tailings Storage Facilities (TSF). Earthquakes are among the most common triggers of tailings dam failures (WISE Uranium Project, 2024). For instance, Villavicencio et al. (2014) reported that 31 out of 38 physical stability failures of Chilean sand tailings dams since 1915, which involved loss of human life, significant environmental damage, and economic losses, were linked to earthquake loading, highlighting the relevance of understanding the seismic response of these geostructures. The seismic response of a tailings dams depends upon the geometry, the stiffness and damping of the materials composing the embankment dam, as well as the input ground motion, among other factors. The stiffness of the materials can be estimated through the shear and compressional wave velocities, which can be measured in-situ with invasive and non-invasive geophysical techniques. The fundamental frequency is another dynamic parameter that characterizes a dam dynamic behavior (Gazetas, 1987). This frequency mainly results from the dam geometry and its material stiffness. An input ground motion with high energy content around the fundamental frequency may induce resonance of the embankment dam, increase its dynamic displacements, and eventually cause slope instabilities, which may compromise the physical stability of the entire TSF.

The most common method to determine the amplification function of a soil deposit is the Standard Spectral Ratio (SSR) method, computed as the spectral ratio between the response at the site of interest with respect to the response of a reference site (Borcherdt, 1970). The reference site must ideally be affected neither by local soil conditions nor by topographic effects. The fundamental frequency is estimated as the lower frequency where the amplification function peaks.

Another simple method that estimates the amplification function is the single-station Horizontal-to-Vertical H/V Spectral Ratio (HVSR) method, also known as the Nakamura's method (Nakamura, 1989). This method was originally developed using continuous records of seismic ambient noise to estimate the soil amplification function and the fundamental frequency of soil deposits (Bard and SESAME-Team, 2004). The HVSR curves can also be obtained from earthquake records (Fernández et al., 2019; Molnar et al., 2018). The validity of the HVSR method has been studied in natural sloped terrains with promising results in the identification of the fundamental frequency (Diaz-Segura, 2016), the estimation of topographic amplification (He et al., 2020), and the presence and orientation of the slope directional resonance (Del Gaudio et al., 2014). Onder Cetin et al., (2005) tested the use of the HVSR method in earthfill dams for water storage and found discrepancies between the fundamental frequencies gathered from the SSR and the HVSR methods attributed to internal impedance contrasts in the dam and 3D valley effects.

This paper analyses the feasibility of estimating fundamental frequencies of a cycloned sand tailings dam located in a highly active seismic region using the HVSR method. The HVSR curves are calculated from seismic ambient noise and earthquakes recorded by a temporal seismic array installed over the dam and the foundation

soil. The results of the HVSRs are compared with SSRs calculated between the crest and the toe of the dam using available earthquake records, including the 2015 Mw 8.3 Illapel Earthquake. More details about this research study can be found in Pastén et al. (2022).

2. Studied sand tailings dam

The studied sand tailings dam is in the Coastal Mountain Range of Central Chile, at about 100 km northwest of Santiago capital city and 25 km from the Pacific coast (Figure 1). It was designed for a maximum storage capacity of $181 \cdot 10^6$ ton of tailings and currently has a 2.7 km^2 footprint (Figure 2a). The embankment dam was built with cycloned sand following the downstream method up to a maximum average height of 60 m, after which the lifting process followed the center-line method at a rising rate of about 2 m/year. The cycloned sand, classified as a silty sand (SM) according to the Unified Soil Classification System (USCS), is hydraulically placed from the crest of the embankment dam towards the downstream slope following a north-south abutment construction sequence. After a 15 cm layer of sand is deposited in the embankment, the layer is compacted with several passes of a mechanical roller compactor to achieve around 90% of the maximum dry density obtained from the Standard Proctor Test. The average dry density of the embankment obtained with this method is approximately 17 ton/m^3 (Valenzuela, 2016). A representative cross-section near the tallest zone of the dam is shown in Figure 2b. The current downstream slope, defined as a horizontal to vertical ratio (H:V), is H:V= 3.5:1, a gentle slope compared to embankment dams built from borrowed materials, which can reach slopes as steep as H:V= 2:1.

Geological reports indicate that the foundation soil contains alluvial soils composed of gravels, clays, and sands. According to borings and test pits, 12-inch boulders can be found in some areas. In other areas, low plasticity clays and clayey sands can be concentrated. Seismic refraction tests and geotechnical borings show that the bedrock depth averages 70 m underneath the crest of the dam, but it can reach up to 90 m near the dam toe. Multi-Channel Analysis of Surface Waves method (MASW) tests performed at the toe of the dam show that the shear wave velocity of the shallower 30 m ranges from 300 to 450 m/s.

The study area is exposed to large interface and intraslab earthquakes. During the last five decades, this region has been affected by the intraslab 1965 Mw 7.4 and the interface 1971 Mw 7.8 La Ligua Earthquakes, the interface 1985 Mw 8.0 Valparaiso Earthquake, and most recently by the interface 2015 Mw 8.3 Illapel Earthquake (Ruiz and Madariaga, 2018).

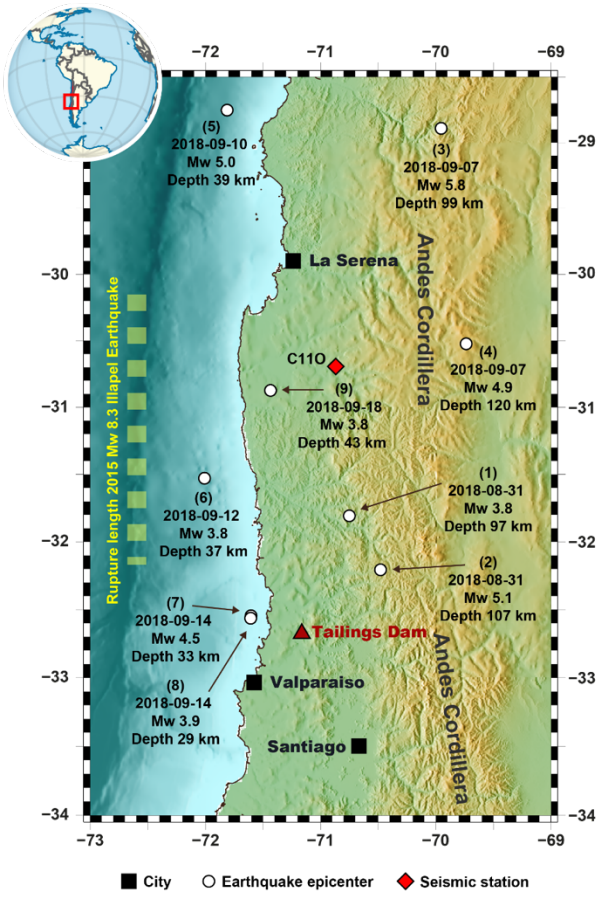

Figure 1. Location of the studied Tailings Dam in Central-North Chile.

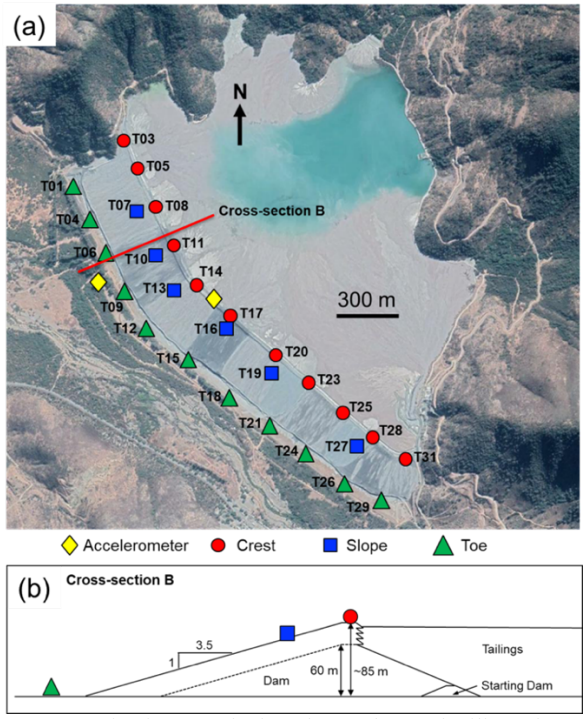

Figure 2. Seismic array deployed over the sand tailings dam. (a) Plan view of the TSF (Google Earth) and (b) cross-section B of the embankment dam. Triangles, circles, and squares represent the location of the temporal array of seismic stations whereas diamonds represent the location of accelerometers that recorded the 2015 Mw 8.3 Illapel Earthquake.

The 2015 Illapel Earthquake (rupture length shown in Figure 1) did not cause damage in the studied tailings dam. Accelerometers installed in the crest and the toe of the embankment (yellow diamonds in Figure 2) recorded maximum horizontal accelerations of 0.11g and 0.06g, respectively (Verdugo et al., 2017). The maximum peak ground acceleration recorded by the National Seismological Center for this earthquake was 0.83 g in the station C11O Monte Patria (Fernández et al., 2019), located 215 km north of the studied tailings dam (see Figure 1).

3. Temporal seismic array

The seismic array installed in the sand tailings dam consisted of 28 stations, each one equipped with a short period 3-component 4.5 Hz geophone, an Omnirecs DataCube3 Ext datalogger recording at 200 Hz, a GPS antenna for time synchronization, and a sealed gel deep cycle battery. The stations recorded continuously from August 29, 2018 to September 26, 2018. Figure 2 shows a plan view with the location of the 28 seismic stations deployed in the tailings dam. Eleven stations were installed in the crest of the embankment dam (red circles in Figure 2), 6 installed in the downstream slope (blue squares in Figure 2), and 11 installed at the downstream slope toe on top of the foundation soil (green triangles in Figure 2). The last group of stations were deployed at an average distance of 5 m apart from the embankment dam due to constraints of the underground infrastructure. The stations were buried in a sealed plastic container and the GPS antennas were raised 50 cm above the surface.

Figure 3 shows an example of the daily continuous record of the station T08 in the vertical component. The amplitude of the velocity time history (Figure 3a) increases during the time of the day when the tailings facility operates, between 9 am and 6 pm. Figure 3b shows a normalized spectrogram with the frequency content of the time history signal. The frequency content remains relatively constant before the operation starts working at the tailings dam (stationary seismic ambient noise in Figure 3a). However, the frequency content changes considerably between 3 and 20 Hz during operation hours.

At least 9 earthquakes of different magnitude were recorded by the seismic stations during the period when the seismic array was under operation. The earthquakes moment magnitudes (Mw) ranged from 3.8 to 5.8 and the epicentral distances vary from 10 to 410 km. The epicenter of the earthquakes along with their dates, magnitudes, and depths are shown in Figure 1 and Table 1.

Figure 4 shows examples of velocity records of Earthquake #7 (Figure 1) in stations located in the crest, the downstream slope, and the toe. The records highlight the amplification of stations in the slope and crest in relation to the strong motion recorded at the toe.

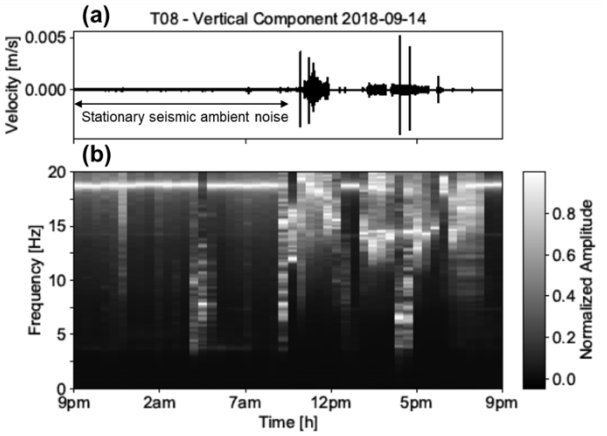

Figure 3. Continuous daily record of station T08 in the vertical component (September 14, 2018). (a) Velocity time history and (b) normalized spectrogram.

Table 1. Recorded Earthquakes

#	Date and time (UTC)	Latitude (°)	Longitude (°)	Depth (Km)	Moment Magnitude (Mw)
1	2018-08-31 10:26:44	-31.811	-70.650	97	3.8
2	2018-08-31 13:25:01	-32.234	-70.489	107	5.1
3	2018-09-07 02:39:17	-28.917	-70.181	99	5.8
4	2018-09-07 23:12:47	-30.470	-69.925	120	4.9
5	2018-09-10 08:24:11	-28.793	-71.547	39	5.0
6	2018-09-12 19:31:14	-31.554	-71.836	37	3.8
7	2018-09-14 18:15:11	-32.524	-71.592	33	4.5
8	2018-09-14 18:46:51	-32.526	-71.592	29	3.9
9	2018-09-18 23:50:10	-30.848	-71.334	43	3.8

SSR calculation consisted of selecting a 2 minutes window centered in the signal maximum amplitude (e.g., see Figure 4). Then, the amplitude Fourier spectra of the velocity records were calculated in each direction and smoothed with a running average window of 0.5 Hz bandwidth. The ratio between the smoothed Fourier amplitudes were computed in the T, L, and vertical directions. Finally, the standard spectral ratios of the analyzed earthquakes were averaged for every station pair.

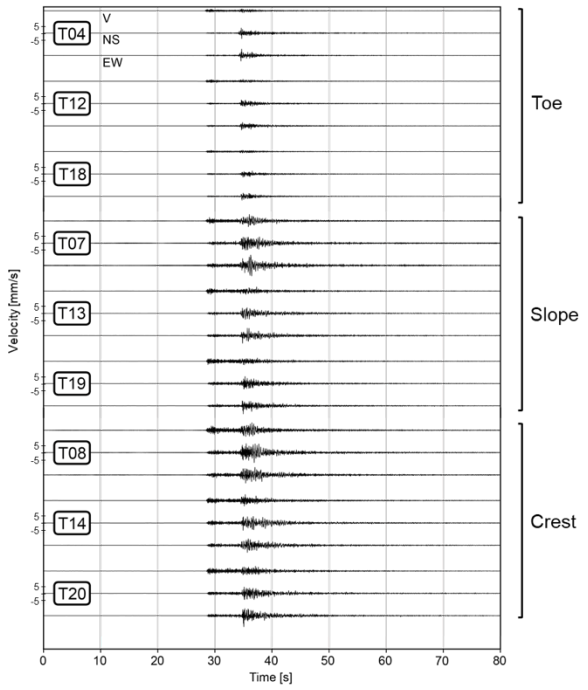

Figure 4. Velocity records of earthquake #7 (epicenter shown in Figure 1 and details in Table 1) in stations located in the crest, the downstream slope, and the dam toe. V: Vertical, NS: North-south, and EW: east-west directions.

3.1. Horizontal to Vertical Spectral Ratios (HVSR)

3.1.1. HVSR from earthquake records (eHVSR)

The earthquakes recorded by the seismic array were used to calculate single-station eHVSR. First, the amplitude Fourier spectra of the velocity records in the T, L, and vertical directions defined for the calculation of the SSR were calculated and smoothed with a running average window of 0.5 Hz bandwidth. Then, the spectra of the horizontal directions (T and L), as well as their square average, were divided by the vertical component. For every evaluated frequency in each station, the mean value was calculated.

3.1.2. HVSR from seismic ambient noise records (mHVSR)

Single-station mHVSR were calculated using 12 hours of stationary seismic ambient noise recorded from 9 pm to 9 am, before the beginning of the TSF operation (Figure 3a). The methodology described in Pastén et al. (2016) was followed, using 30 s windows automatically selected from the amplitude STA/LTA ratio between 0.5 and 2.0, with a short time period t_{STA} = 1 s, and a long time period t_{LTA} = 60 s. The horizontal component was calculated as the squared average of the T and L directions in the frequency domain. The calculations were performed using the open-source Geopsy software (www.geopsy.org).

4. Results

Figure 5 shows an example of the SSR computed for the station pair T14-T12 in the L, T, and vertical directions. The thick curve was computed as the average of the six recorded earthquakes (see the earthquakes considered in Table 3). Both horizontal directions (L and T) show similar amplification patterns with peak amplitudes at about 0.9 Hz, whereas the vertical direction has the largest amplification at 1.85 Hz, nearly twice the horizontal peak vibration frequency. The peak SSR amplitudes at the fundamental frequencies are about eight in the L, T, and vertical directions.

Table 2. Station pairs and earthquakes considered in the calculation of SSR

	Earthquake								
Station Pair	**1**	**2**	**3**	**4**	**5**	**6**	**7**	**8**	**9**
T05-T01	Y	Y	Y	Y	Y				
T08-T04	Y	Y	Y		Y	Y	Y	Y	
T11-T09	Y	Y	Y	Y	Y	Y	Y	Y	
T14-T12			Y	Y	Y	Y	Y	Y	
T17-T15			Y	Y	Y	Y	Y	Y	Y
T20-T18			Y	Y	Y	Y	Y	Y	Y
T23-T21	Y	Y				Y	Y	Y	Y
T25-T24	Y	Y	Y	Y	Y	Y	Y	Y	Y
T28-T26			Y	Y	Y		Y	Y	Y
T31-T29			Y	Y			Y	Y	Y
T07-T06			Y	Y	Y	Y	Y		
T13-T12			Y	Y	Y	Y	Y	Y	
T16-T15			Y	Y	Y	Y	Y	Y	Y
T19-T18			Y	Y	Y	Y	Y	Y	Y
T27-T26			Y	Y	Y		Y	Y	Y

Note: "Y" means that the earthquake was recorded by the station pair

The SSR in the horizontal directions (Figure 5a and 5b) show a second peak at about 3 Hz, which could be associated to the second harmonic mode of the earth structure. Note that the ratio between 3 Hz and the fundamental frequency at 0.9 Hz is about 3:1, similar to the ratio between the frequencies of the second and the first harmonics of a single horizontal soil layer predicted by the one-dimensional shear wave propagation theory (Roesset, 1977).

Figure 6 shows examples of eHVSR computed for the stations T12, T13, and T14 located along a cross-section near the direction change of the crest axis (Figure 2). The peak frequency of station T12 at the dam toe is 1.7 Hz with an average peak amplitude close to five (Figure 6a). In contrast, the peak frequency of the sensor T14 over the crest is 0.95 Hz with an average peak amplitude near seven (Figure 6c). This peak frequency is similar to that found in the SSR computed for the station pair T14-T12 in the longitudinal and transverse directions (Figure 5a and 5b). The eHVSR of the sensor located in the downstream slope shows two peaks at about 0.9 and 1.1 Hz (Figure 6b). The nature of these peaks will be addressed in the Discussion section.

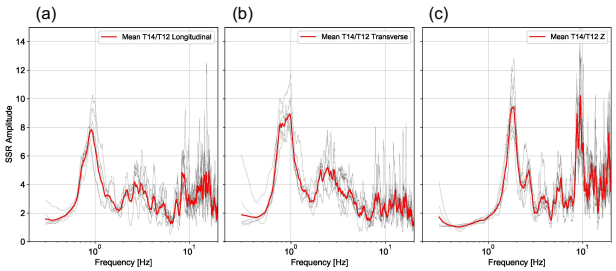

Figure 5. SSR computed for the station pair T14-T12 in the (a) longitudinal, (b) transverse, and (c) vertical directions.

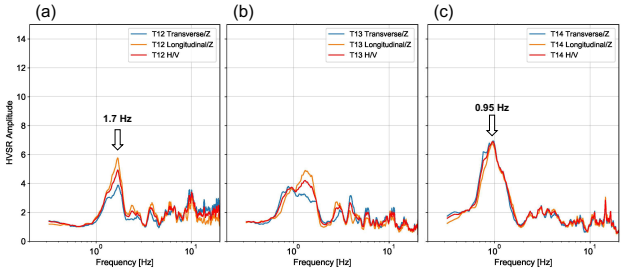

Figure 6. eHVSR computed for the stations (a) T12 (toe), (b) T13 (downstream slope), and (c) T14 (crest) in the T and L directions.

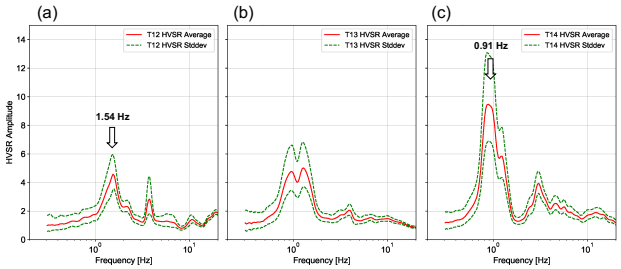

Figure 7. Average mHVSR computed for the stations (a) T12 (toe), (b) T13 (downstream slope), and (c) T14 (crest).

Figure 7 shows mHVSR calculated in the same stations analyzed in Figure 6. The shape of the curves, the peak frequencies and peak amplitudes are similar to those obtained with earthquake records. Moreover, the peak frequencies of the station in the crest T14 are similar to the frequencies found in the SSR (Figure 5a and 5b). The second peak at about 3 Hz found in T14 (Figure 7c) is similar to that found in the SSR of the same station (Figure 5a and b), which could be associated to the second harmonic mode of the earth structure. The mHVSR at the station T13 also has two peaks around 1 Hz.

Figure 8 compares the average peak frequencies obtained from eHVSR and mHVSR for all the individual stations shown in Figure 2a. The results are shown for the transverse (filled symbols) and longitudinal directions (open symbols). Peak frequencies obtained from eHVSR and mHVSR in the crest and the downstream slope are similar in a wide range of frequencies between 0.8 and 1.6 Hz although eHVSR peak frequencies tend to exceed those from mHVSR. The larger variability in the peak frequencies obtained from eHVSR may be due to the few earthquakes analyzed compared to the longer records of seismic ambient noise considered for the calculation of mHVSR. Stations with two peaks in the SSR and HVSR (e.g., T05 and T19) and stations near the abutments (e.g., T01, T03, T04, T29, and T31) have the largest differences between eHVSR and mHVSR peak frequencies.

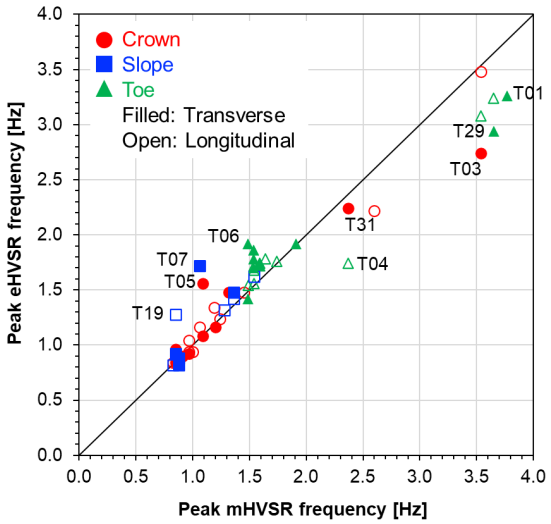

Figure 8. Comparison of peak frequencies of the seismic stations in Figure 2 obtained from eHVSR and mHVSR.

Figure 9a shows the variation of the peak frequency of mHVSR along the longitudinal embankment dam axis considering the distance from the north abutment. Stations at the dam toe over the foundation soil tend to have peak frequencies of about 1.5 Hz in the central part of the dam from 450 m to 1,900 m of the north abutment. Similarly, the peak frequencies of stations either along the crest or the downstream slope tend to have values between 0.9 and 1.1 Hz from 350 m to 1,500 m from the north abutment. The fundamental frequencies in stations in the crest and the dam toe increase drastically near the abutments. The figure also shows that the SSR peak frequencies in the central part of the dam agree with the mHVSR peak frequencies. Note that SSR of stations near the abutments are not presented in the figure.

Figure 9b shows the changes in peak frequencies obtained from the mHVSR and SSR, as well as the dam height and the thickness of the foundation sediment along the dam crest. The sediment thickness in the foundation soil deposit was estimated from geological reports developed prior the construction of the tailings dam whereas the dam height was estimated from as-built blueprints. The relatively constant fundamental frequencies measured by the stations over the crest in the central part of the dam (from 350 m to 1,500 m of the north abutment) is related to a zone where the total thickness, calculated as the sum of the dam height and the sediment thickness, remains approximately constant at 140 m. A similar trend is observed in the frequencies calculated from the stations in the toe from 450 m to 1900 m of the north abutment. In contrast, the fundamental frequencies in stations near the abutments, both in the crest and the toe, increase drastically as the sediment thickness decreases. The peak frequencies in stations in the downstream slope are similar to those at the crest but some stations exhibit different peak frequencies in the longitudinal and transverse directions (e.g., T07 and T13).

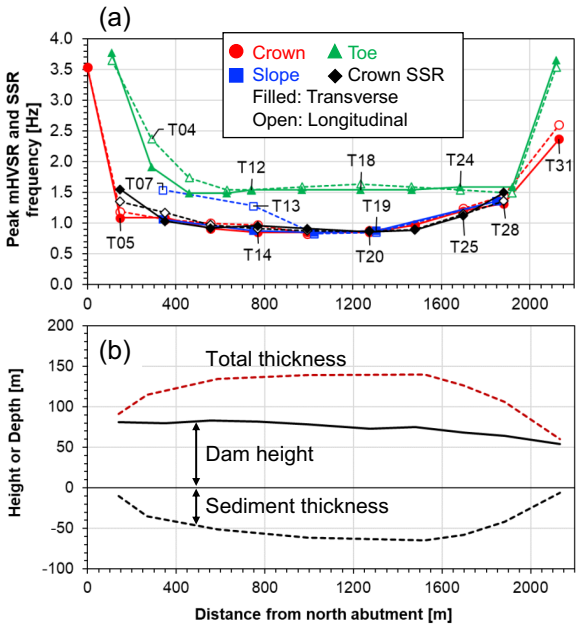

Figure 9. (a) Peak frequencies obtained from SSR and mHVSR evaluated in the crest, slope, and dam toe, compared to (b) the height of the embankment and the sediment thickness along the dam crest. Total thickness is the sum of the dam height and the sediment thickness.

The fundamental frequency over the embankment dam is lower than that over the toe because the thickness of the underlying sediment at the toe is smaller than the material below the stations at the crest. In general, the amplitudes of the mHVSR and eHVSR in the crest are larger than the amplitudes at the toe (as shown in Figures 6 to 7).

5. Discussion

Figure 10a shows a shear-wave profile representative of the tallest dam section from the crest to the foundation soil (see Figure 2b). The Vs profile follows the expression proposed by Gazetas (1982) for earth dams

$$V_s(z) = V_{sb}\left[\frac{z+h}{H+h}\right]^{1/3}; 0 < z < H \qquad (1)$$

Where H= 85 m is the height of the dam section (i.e., the height of a truncated wedge) and V_{sb}= 360 m/s is the maximum shear-wave velocity at the base of the dam, considering a truncation ratio λ= h/(H+h)= 0.05 (h=4.475 m is the distance from the truncated tip to the imaginary intersection between the downstream and upstream slopes of the wedge). The shallower 40 m of the Vs-profile in Figure 10a fits the lower-bound velocities obtained from 30 Vs profiles obtained with the MASW method and 7 Vs profiles obtained from seismic cone penetration tests (sCPT) performed in the dam. The upper and lower bounds of these Vs profiles are shown in Figure 10a.

Figure 10b shows the theoretical transfer function of a 1D soil column with the shear wave velocity profile shown in Figure 10a, a density of 1.7 ton/m^3, and a constant critical damping ratio of 2% when it is subjected to a vertically incident SH-wave (Roesset, 1977). The model assumes that the substrate of the dam has a shear-wave velocity Vsr= 1,000 m/s, a density of 2.2 ton/m^3, and a damping ratio of 2%. The fundamental frequency of the 1D model is f= 0.92 Hz, similar to the frequencies found from SSR and HVSR around station T14 in the central part of the dam (see Figures 5, 6, and 7). The amplitude of the theoretical transfer function is about half that of the empirical SSR.

On the other hand, for small values of the truncation ratio λ, the fundamental frequency of either a homogeneous or an inhomogeneous two-dimensional truncated wedge can be approximated by (Gazetas, 1982)

$$f_0 = \frac{V_{sb}}{3(H+h)} \qquad (2)$$

Evaluating Eq. 2 for H= 85 m, h=4.475 m, and V_{sb}= 360 m/s yields a fundamental frequency f_0= 1.34 Hz.

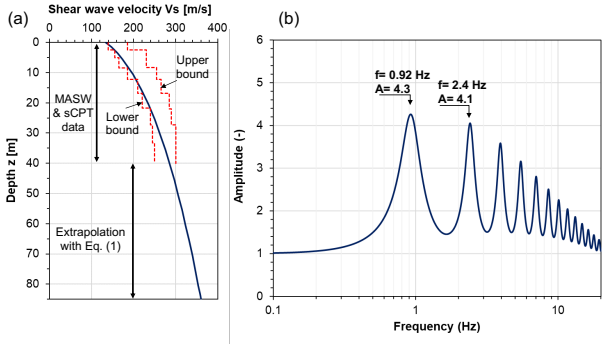

Figure 10. (a) Shear-wave velocity profile representative of the tallest section of the dam. (b) 1D SH-wave transfer function.

These results suggest that the fundamental frequency of a tailings embankment dam with a gentle downstream slope, such as that analyzed in this study, may be estimated in the central part, away from the abutments, from the theoretical transfer function of a 1D soil column that extend from the dam crest to the foundation soil.

This preliminary conclusion may be valid for small magnitude earthquakes. To test its validity for larger earthquakes, the records from the 2015 Mw 8.3 Illapel Earthquake gathered from GeoSig GSR AC-63 triaxial force balance accelerometers were analyzed. The peak ground accelerations recorded in the crest sensor were 0.11 g, 0.09 g, and 0.07 g in the transverse, longitudinal, and vertical directions, respectively. The peak ground accelerations recorded in the base sensor were 0.05 g, 0.06 g, and 0.03 g in the transverse, longitudinal, and vertical directions, respectively. The location of the sensors in the crest and the base of the dam are shown in Figure 2.

Figure 11a shows SSRs obtained as the ratio between the records in the crest and the base in the three directions. The fundamental frequencies obtained from the SSR are about 0.9 Hz in both horizontal directions and about 1.8 Hz in the vertical direction. Similar horizontal fundamental frequencies are found processing the earthquake records as eHVSR (Figure 11b). These values agree with the frequencies obtained for the central part of the embankment from SSR and mHVSR (see Figure 9a).

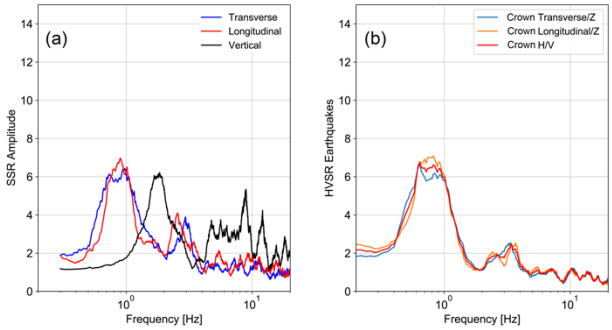

Figure 11. (a) SSR and (b) eHVSR at the dam crest calculated from records of the 2015 Illapel Earthquake. The location of the accelerometer is shown in Figure 2a.

6. Conclusions

The results from the mHVSR and eHVSR are consistent and show that:

- the foundation soil is stiffer than the embankment dam,
- the fundamental frequency of the dam is about 0.9 Hz in the central part away from the abutments, and
- there are different predominant vibration frequencies along the downstream slope and along the crest axis from the north to south abutment.

The results of the HVSR were compared with SSR calculated between the crest and the dam toe using the available earthquake records. Both methods are consistent in terms of the fundamental frequency and amplification factors.

The agreement between mHVSR, eHVSR, and SSR improves in the central part of the dam, approximately 400 m away from the abutments. More complex seismic amplification patterns and seismic wave reflection may develop near the abutments due to abrupt changes in the dam height and sediment thickness in the foundation soil. The difference between SSR and HVSR could help identifying zones of the dam that can be studied with 2D approaches, such as 2D numerical simulations, from zones near the abutments of the dam that must be analyzed with 3D methods.

The fundamental frequency obtained from HVSR and SSR in the central part of the dam with gentle downstream slope can be approximated by the value obtained from the 1D SH-wave propagation theory, considering a soil column from the dam crest to the interface with the foundation soil.

Acknowledgements

Support for this research was provided by the Advanced Mining Technology Center (AMTC PIA ANID grant AFB230001) and by the ANID FONDECYT Grant Nº1240744.

References

Bard, P.-Y., SESAME-Team, 2004. Guidelines for the Implementation of the H / V Spectral Ratio Technique on Ambient Vibrations Measurements , Processing and Interpretation. https://doi.org/DOI 10.1111/j.1365-246X.2006.03282.x

Borcherdt, R.D., 1970. Effects of Local Geology on Ground Motion Near San Francisco Rbay. Bull. Seismol. Soc. Am. 60, 29–61.

Del Gaudio, V., Muscillo, S., Wasowski, J., 2014. What we can learn about slope response to earthquakes from ambient noise analysis: An overview. Eng. Geol. 182, 182–200. https://doi.org/10.1016/j.enggeo.2014.05.010

Diaz-Segura, E.G., 2016. Numerical estimation and HVSR measurements of characteristic site period of sloping terrains. Géotechnique Lett. 6, 176–181. https://doi.org/10.1680/jgele.16.00009

Dobry, R., Alvarez, L., 1967. Seismic Failures of Chilean Tailings Dams. J. Soil Mech. Found. Div. 93, 237–260. https://doi.org/10.1061/jsfeaq.0001054

Fernández, J., Pastén, C., Ruiz, S., Leyton, F., 2019. Damage assessment of the 2015 Mw 8.3 Illapel earthquake in the North-Central Chile. Nat. Hazards 96, 269–283. https://doi.org/10.1007/s11069-018-3541-3

Gazetas, G., 1987. Seismic response of earth dams: some recent developments. Soil Dyn. Earthq. Eng. 6, 2–47. https://doi.org/10.1016/0267-7261(87)90008-X

Gazetas, G., 1982. Shear vibration of vertically inhomogeneous earth dams. Int. J. Numer. Anal. Methods Geomech. 6, 219–241. https://doi.org/10.1002/nag.1610060208

He, J., Qi, S., Wang, Y., Saroglou, C., 2020. Seismic response of the Lengzhuguan slope caused by topographic and geological effects. Eng. Geol. 265, 105431. https://doi.org/10.1016/j.enggeo.2019.105431

Molnar, S., Cassidy, J.F., Castellaro, S., Cornou, C., Crow, H., Hunter, J.A., Matsushima, S., Sánchez-Sesma, F.J., Yong, A., 2018. Application of Microtremor Horizontal-to-Vertical Spectral Ratio (MHVSR) Analysis for Site Characterization: State of the Art. Surv. Geophys. 39, 613–631. https://doi.org/10.1007/s10712-018-9464-4

Nakamura, Y., 1989. A method for dynamic characteristics estimation of subsurface using microtremor on the ground surface. Q. Reports Railw. Tech. Res. Inst. 30, 25–33.

Onder Cetin, K., Isik, N.S., Batmaz, S., Karabiber, S., 2005. A comparative study on the actual and estimated seismic response of kiralkizi dam in turkey. J. Earthq. Eng. 9, 445–460. https://doi.org/10.1080/13632460509350550

Pastén, C., Sáez, M., Ruiz, S., Leyton, F., Salomón, J., Poli, P., 2016. Deep characterization of the Santiago Basin using HVSR and cross-correlation of ambient seismic noise. Eng. Geol. 201, 57–66. https://doi.org/10.1016/j.enggeo.2015.12.021

Pastén, C., Peña, G., Comte, D., Díaz, L., Burgos, J., and Rietbrock, A. (2022). On the use of the H/V spectral ratio method to estimate the fundamental frequency of tailings dams. Journal of Earthquake Engineering, 27(6), 1649-1664, 10.1080/13632469.2022.2087799

Roesset, J.M., 1977. Soil amplification of earthquakes, in: Desai, C.S., Christian, J.T. (Eds.), Numerical Methods in Geotechnical Engineering. McGraw Hill.

Ruiz, S., Madariaga, R., 2018. Historical and recent large megathrust earthquakes in Chile. Tectonophysics 733, 37–56. https://doi.org/10.1016/j.tecto.2018.01.015

Valenzuela, L., 2016. Design, construction, operation and the effect of fines content and permeability on the seismic performance of tailings sand dams in Chile. Obras y Proy. 19, 6–22.

Verdugo, R., Peters, G., Campaña, J., Valenzuela, L., Bard, E., 2017. Evaluation of Tailings Dams Subjected to Large Earthquakes, in: Proceedings of the 19th International Conference on Soil Mechanics and Geotechnical Engineering, Seoul, Korea. pp. 1615–1618.

Villavicencio, G., Espinace, R., Palma, J., Fourie, A., Valenzuela, P., 2014. Failures of sand tailings dams in a highly

seismic country. Can. Geotech. J. 51, 449–464. https://doi.org/10.1139/cgj-2013-0142

WISE Uranium Project 2024. Chronology of major tailings dam failures, World Information Service on Energy Uranium Project, accessed February 6, 2024, http://www.wise-uranium.org/mdaf.html